



Universiteit  
Leiden

The Netherlands

## Pushing the characterization of exoplanet atmospheres down to temperate rocky planets in the era of JWST

Zieba, S.

### Citation

Zieba, S. (2024, June 25). *Pushing the characterization of exoplanet atmospheres down to temperate rocky planets in the era of JWST*. Retrieved from <https://hdl.handle.net/1887/3765836>

Version: Publisher's Version

License: [Licence agreement concerning inclusion of doctoral thesis in the Institutional Repository of the University of Leiden](#)

Downloaded from: <https://hdl.handle.net/1887/3765836>

**Note:** To cite this publication please use the final published version (if applicable).

# 1

## INTRODUCTION

### 1.1 Exoplanet Population

The story of this thesis starts in the year 1995: By detecting a periodic shift in the spectral lines of the sun-like star 51 Pegasi, Michel Mayor and Didier Queloz concluded that the star was being orbited by a Jupiter-mass planet (Mayor & Queloz 1995). The most surprising aspect of this discovery was the orbital period of the planet; 51 Pegasi b orbited its host star every 4.2 days. This is far shorter than the period for any Solar System planet. The first gas giant as seen from the Sun, Jupiter, needs approximately a thousand times longer to complete one revolution around our Sun. For this discovery, the two astronomers were eventually awarded with the Nobel Prize in Physics in 2019.

Since this first discovery of an exoplanet around a Sun-like star nearly 30 years ago, the field has progressed considerably. Based on data retrieved from the NASA Exoplanet Archive at the end of 2023, over 5500 exoplanets were detected to this day (see Figure 1.1). Main findings of the past few decades include: (a) small planets being a common outcome of planet formation (see Chapter 1.1.1), (b) the prediction and discovery of the so-called Radius Valley, a lack of planets with approximately two times the Earth’s radius, and (c) the existence of planets on “ultra-short-orbits” ( $< 1$  day) (see Chapter 1.1.2). In this Introduction, I will present these various planet populations focusing on smaller exoplanets. With the advent of *JWST*, we can characterize rocky exoplanets in detail like never before. In fact, 35 of the 116 transiting exoplanets that will be observed in Cycles 1 and 2 of *JWST* are small planets ( $< 2 R_{\oplus}$ , with  $R_{\oplus}$  being Earth’s radius) to study their atmospheres or surfaces. In Chapter 1.2, I explain the main techniques to characterize transiting exoplanets. Some noteworthy systems and planets are presented in Chapter 1.3. The space-based workhouse facilities for the study of small exoplanets are discussed in Chapter 1.4. Finally, in Chapter 1.5, I introduce the individual scientific chapters of this thesis and their main conclusions.

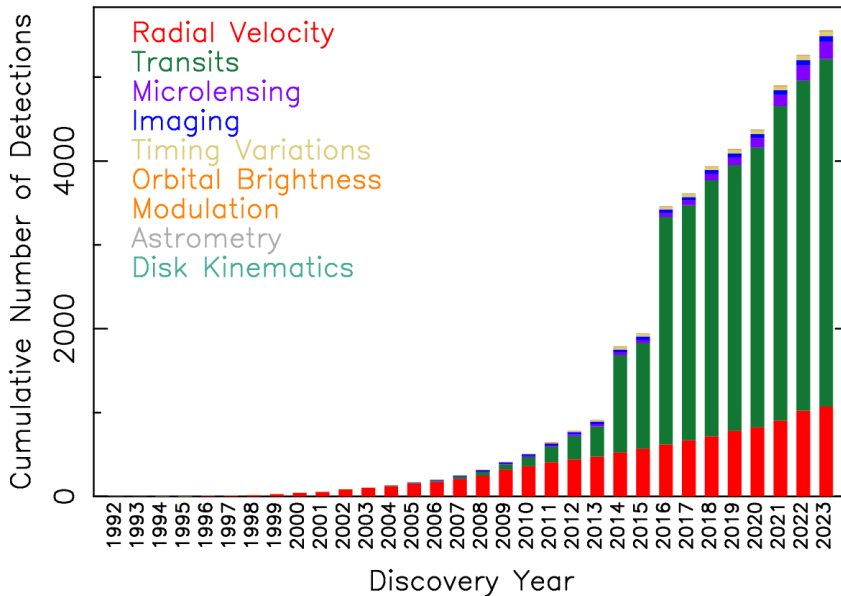


**Figure 1.1:** Plot showing the cumulative number of detected exoplanets as a function of time. From the first detection of planets around a pulsar (Wolszczan & Frail 1992), progressing to the detection of a hot Jupiter orbiting a solar-like star in 1995 (Mayor & Queloz 1995), and the multitude of transiting exoplanets unveiled during the early 2010s by NASA’s *Kepler Space Telescope* (Borucki et al. 2010), we know of more than 5500 exoplanets to date. Retrieved from the NASA Exoplanet Archive in December 2023.

### 1.1.1 Rocky exoplanets

Thanks to the many dedicated exoplanet missions of the past, like NASA’s *Kepler Space Telescope*, which has discovered approximately half of all the exoplanets known today, we know that planets are ubiquitous in our Galaxy (Dressing & Charbonneau 2015; Fulton et al. 2017; Zhu & Dong 2021). The formation of planets commonly yields small exoplanets, and they are even more prevalent around smaller stars (Rogers 2015; Fulton et al. 2017). By measuring their masses and radii, we learned that planets smaller than  $1.6 R_{\oplus}$  are most likely terrestrial (i.e., rocky) in composition (Weiss & Marcy 2014; Rogers 2015; Wolfgang & Lopez 2015). In Figure 1.2, mass and radius measurements of exoplanets are shown compared to a range of compositional scenarios (Wordsworth & Kreidberg 2022). Smaller planets usually fall into two bounding cases that characterize rocky planets: those composed of 100% iron and those made up of 100% silicates ( $\text{MgSiO}_3$ ). All of the terrestrial Solar System planets can be found between these two extremes, with Earth showing a composition of approximately 30% iron and 70% silicates. Above  $1.6 R_{\oplus}$ , exoplanets show a bigger spread in radii for a given mass and deviate from this rocky regime. These planets need a significant fraction of their mass in gas or volatiles, like hydrogen ( $\text{H}_2$ ) or water ( $\text{H}_2\text{O}$ ). Even a small amount of hydrogen - just 1% by mass - in the atmosphere of a small planet,

leads to a significant increase in its radius of  $2 R_{\oplus}$  (Valencia et al. 2010; Lopez & Fortney 2014). Their envelope then contributes a significant fraction to the size of the planet. Thinner atmospheres are not expected as they are very vulnerable to escape processes and easily lost by stellar wind. Furthermore, planets with 1% of their mass in a hydrogen-dominated envelope, are not expected to have solid, rocky surfaces. Due to the high pressures and temperatures, their surfaces are expected to be molten (Lopez & Fortney 2014; Chachan & Stevenson 2018). All of this is essentially why we typically do not consider these planets with primordial, hydrogen atmospheres to be rocky. Another major observation made by data collected by the *Kepler* mission is the drought of planets ranging between 1.5 and 2.0 Earth radii. The phenomenon, referred to as the radius valley or radius gap, is likely attributed to the rapid increase in planet size when a thick gaseous atmosphere persisted (Fulton et al. 2017; Van Eylen et al. 2018).

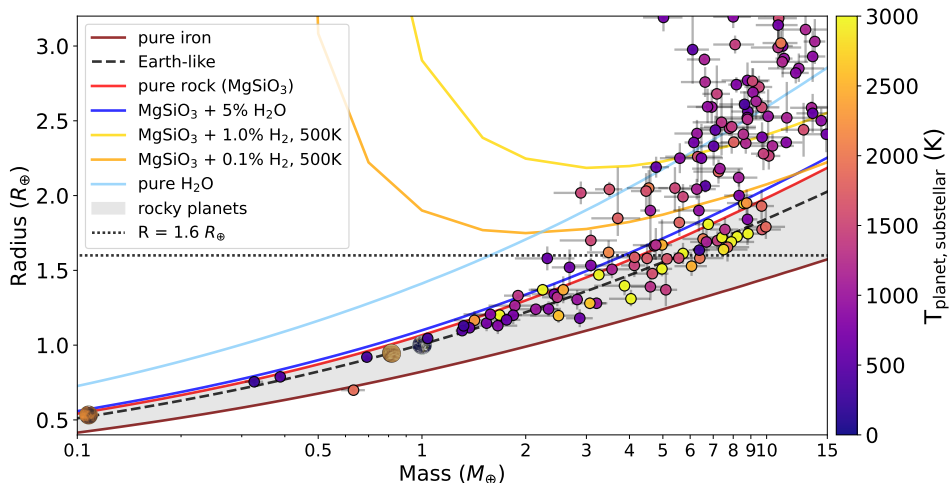


**Figure 1.2:** A mass-radius diagram comparing discovered exoplanets compared to a suite of compositional models. The gray shaded area shows the region in the mass-radius parameter space which is typically identified as being rocky. It is enclosed by two compositional lines: the 100% iron (Fe) model (brown solid line) and the pure rock or silicate line (100%  $\text{MgSiO}_3$  in solid red). The Earth-like compositional line consists of 32.5% iron and 67.5% silicates. Other models with various amounts of volatiles are also shown. The horizontal dotted line depicts a radius of 1.6 Earth Radii ( $R_{\oplus}$ ), above which planets are predicted to retain a substantial hydrogen atmosphere (Rogers 2015). The confirmed planets are color-coded by their substellar temperatures defined by  $T_{\text{subst}} = T_{\text{eff}} / \sqrt{a/R_s}$ , with  $T_{\text{eff}}$  being the effective temperature of the host star and  $a/R_s$  the semi-major-axis to stellar radius ratio. We also show the images of the Solar System planets Mars, Venus, and Earth in the plot in their corresponding positions in this mass-radius plot. For clarity, we only show discovered exoplanets, which have at least a  $5\sigma$  mass and radius detection. The plot was adapted and updated from Wordsworth & Kreidberg (2022). The planetary parameters were accessed from the NASA Exoplanet Archive in December 2023. The compositional lines were taken from Zeng et al. (2019).

Even though we have discovered many small exoplanets to this day, and we expect them to be rocky in composition based on their measured bulk densities, we still only have little knowledge about the makeup of their atmospheres (for a recent review on rocky exoplanet atmospheres see Wordsworth & Kreidberg 2022). Our solar system already exhibits a diverse range of atmospheres for rocky bodies (see Figure 1.3): Venus with its thick (93 bar) CO<sub>2</sub> dominated atmosphere, Saturn’s moon Titan with an N<sub>2</sub> dominated one at 1.5 bar, Earth with its 1 bar atmosphere predominantly composed out of N<sub>2</sub> and O<sub>2</sub>, and Mars with its thinner (0.006 bar) CO<sub>2</sub>-dominated atmosphere (for a review on these thicker Solar System atmospheres see Encrenaz & Coustenis 2018). Our Solar system also contains planets with thin, tenuous atmospheres: Pluto and Neptune’s moon Triton have N<sub>2</sub> as their main atmospheric species and a surface pressure of the order of 10 microbars caused by the sublimation of ices. Jupiter’s moon Io has an SO<sub>2</sub> nanobar atmosphere generated by sublimation and vulcanism. Mercury is too close to the Sun to hold onto any significant atmosphere. Its exosphere is created by captured solar wind particles and by meteors hitting the planetary surface. It has a thickness of approximately 1 picobar (10<sup>-12</sup> bars) and is mainly composed of hydrogen, helium, oxygen, sodium, potassium, and calcium (Domingue et al. 2007) (for a review of these tenuous solar system atmospheres see Lellouch 2018).

The theoretical prediction of an atmosphere on small planets also remains challenging due to numerous unknown factors, which can affect its composition and thickness, such as atmospheric escape, outgassing from volcanism, the delivery of volatiles by comets, rainout, and the existence of plate tectonics (e.g., Raymond et al. 2004; Kite et al. 2009; Wordsworth 2015; Luger & Barnes 2015; Bolmont et al. 2017; Moore & Cowan 2020). The spectral type of the host star may also strongly influence a planet’s atmosphere. M-dwarf stars provide their planets with a completely different environment than Sun-like stars. These stars undergo prolonged pre-main sequence phases marked by heightened luminosity (Luger & Barnes 2015) and also show increased starspot activity leading to increased XUV radiation (France et al. 2016; McDonald et al. 2019). Additionally, M-dwarfs exhibit heightened coronal-mass-ejection activity than their solar-like counterparts (Crosley & Osten 2018; Odert et al. 2020). Despite all of that, planets around M dwarfs remain the easiest to study. Their proximity to their host stars results in a greater transit probability and the relatively high planet-to-star radius ratio leads to a higher signal-to-noise of the planet’s atmospheric features making them easiest to be studied. Therefore, M dwarfs, being the most prevalent type of stars in the galaxy, offer a large sample of planets with high signal-to-noise exoplanets to characterize. These advantageous aspects are commonly referred to in the exoplanet community as the “M-dwarf opportunity”.

### 1.1.2 Ultra-short-period planets

After the discovery of 51 Pegasi b on its 4.2 day orbit, even more extreme planets were discovered. In 2009, the *CoRoT* (Convection, Rotation and Transits) telescope detected CoRoT-7 b, a planet with a radius of 1.7  $R_{\oplus}$  and an orbital period of just 20 hours (Léger et al. 2009). At the time of its discovery, it was the small-

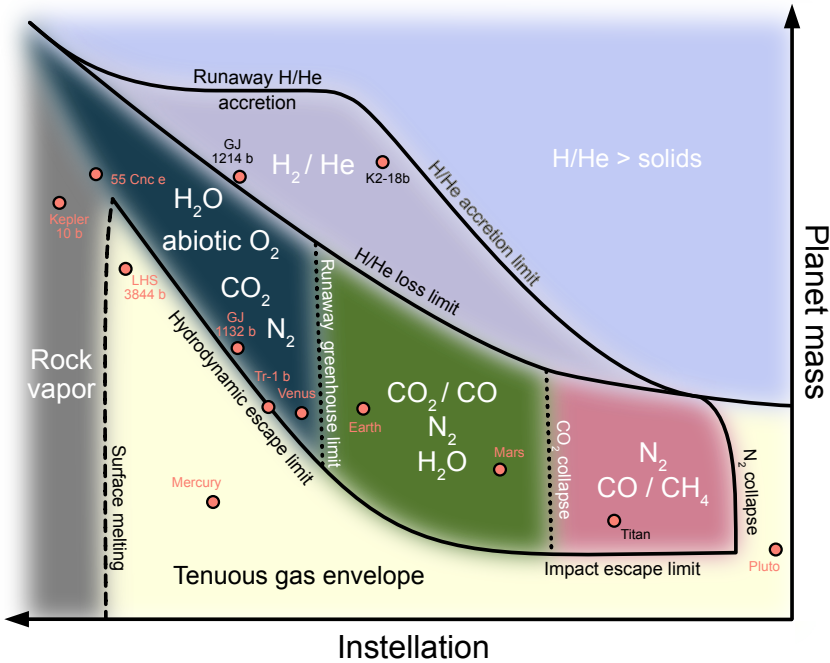


**Figure 1.3:** A regime plot showing various atmospheric scenarios for a range of stellar instellations and planetary masses. Planets with high masses are expected to have retained their hydrogen/helium-dominated atmospheres (we typically do not consider them as being “rocky”). Low-mass planets and more irradiated planets suffer from atmospheric escape and might be bare rocks (e.g., Mercury in the Solar System). Very high irradiated planets (lava planets) are expected to develop a rock vapor atmosphere. Substantial high-mean-molecular weight atmospheres (e.g.,  $\text{CO}_2$ ,  $\text{H}_2\text{O}$ ,  $\text{O}_2$ ,  $\text{N}_2$ ) can be found in the dark blue, green, and pink areas. Various exoplanets and Solar System planets are marked as red dots in the plot for comparison. Figure taken from Lichtenberg et al. (2023).

est planet found up to that point and had the shortest period. By convention, we call these exoplanets with orbital periods shorter than a day “ultra-short-period” planets (also known as “USPs”) (for a review on these USPs, see Winn et al. 2018). The majority of these strongly irradiated worlds are smaller than  $2.0 R_{\oplus}$  (Sanchis-Ojeda et al. 2014; Jontof-Hutter 2019). Being on these tight orbits, the tidal forces experienced by the planet translate into a very short circularization time scale leading to quick attenuation of any non-zero eccentricity and also giving it a permanent dayside and nightside (Winn et al. 2018). From theoretical and empirical work on these USPs we can therefore assume that they are tidally locked (Lyu et al. 2023).

USPs, just like hot Jupiters, are not common in the Milky Way (Cumming et al. 2008; Wright et al. 2012; Winn et al. 2018). By determining the occurrence rate of USPs, Sanchis-Ojeda et al. (2014) found that only one out of 200 G-type stars have

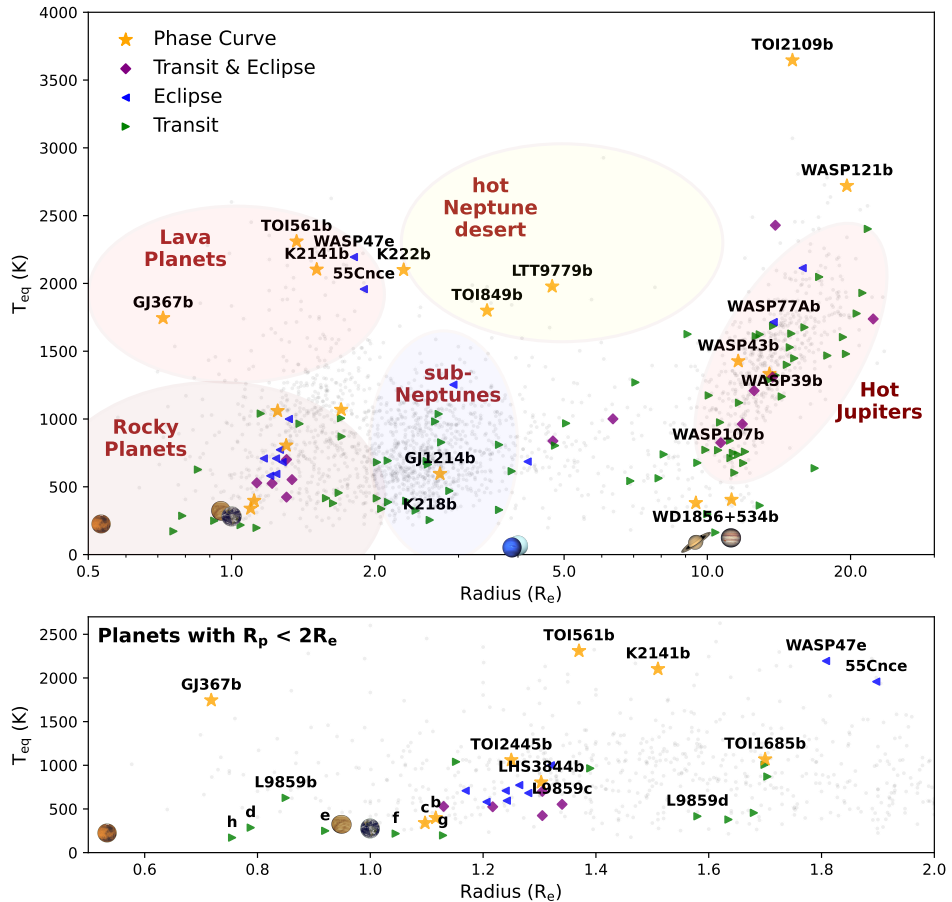


**Figure 1.4:** The exoplanet “zoo” showing the equilibrium temperature of all confirmed planets (gray dots) as a function of their radius. The equilibrium temperature  $T_{\text{eq}}$  assumes perfect reradiation of heat and a Bond albedo of zero:  $T_{\text{eq}} = T_{\text{eff}} / \sqrt{2a/R_s}$ , with  $T_{\text{eff}}$  being the effective host star temperature and  $a/R_s$  the semi-major-axis to stellar radius ratio. We mark the rough location of prominent exoplanet populations and show the images of the Solar System planets in the plot in their corresponding positions in this temperature-radius plot (Mercury with approximately  $0.4 R_{\oplus}$  is not shown). The names of noteworthy exoplanets, discussed in any scientific chapters, or well-studied planets, have been positioned above the corresponding dots on the plot. Planets observed by *JWST* in Cycle 1 or 2 are additionally highlighted: those set for phase curve observations with a yellow star ( $\star$ ), eclipse observations with a blue left-pointing triangle ( $\blacktriangleleft$ ), transit observations with a green right-pointing triangle ( $\blacktriangleright$ ), and both with purple diamonds ( $\blacklozenge$ ). The lower panel provides a zoom-in to the population of smaller exoplanets but is otherwise identical to the upper panel.

a planet on such a tight orbit (see also Bryson et al. 2020; Zhu & Dong 2021). For comparison, one in five G-type stars are estimated to have an Earth-sized planet

in the habitable zone around their stars (Kunimoto & Matthews 2020). The origin of these USPs is still being highly studied and the dominant formation mechanism is generally unknown.

USPs are typically small: of the 132 planets discovered to this date with an orbital period shorter than a day and a measured radius, 113 (i.e., 86%) are smaller than 2 Earth radii. For comparison, only 37% (1562 of 4180) of all planets with radii are  $< 2 R_{\oplus}$ . It was originally thought that these small USPs might have been Hot Jupiters (HJs) which underwent photoevaporation due to the proximity to their host star (Jackson et al. 2013; Valsecchi et al. 2015; Königl et al. 2017; Winn et al. 2018). However, two observations have emerged, suggesting otherwise. Firstly, it is well known that HJs are typically found around metal-rich stars (Petigura et al. 2018). This strong correlation with metallicity is not seen for small USP planets (Winn et al. 2017). If HJs would have been the progenitors of USPs then they also have to orbit the same type of stars. Secondly, HJs are typically found alone and rarely have other planets in their systems. This is in strong contrast to USPs which often have other companions in the system (Sanchis-Ojeda et al. 2014; Adams et al. 2017; Petrovich et al. 2019). This still leaves sub-Neptunes as a possible progenitor. In this scenario, small USPs would be exposed cores of sub-Neptunes (planets with approximately  $2.0 - 3.9 R_{\oplus}$ ) instead which underwent photoevaporation or Roche overflow (Lundkvist et al. 2016; Lee & Chiang 2017; Winn et al. 2018). This would then be also consistent with hot-sub Neptunes not showing a strong correlation with host star metallicity like USPs (Winn et al. 2018). In this scenario, the progenitors might have initially formed at greater separations and then migrated to their current orbits due to gravitational interactions with the disk (Ida & Lin 2004; Schlaufman, Lin & Ida 2010; Terquem 2014) or tidal dissipation (Petrovich et al. 2019; Pu & Lai 2019). As the planets would have formed further out then, they would consist of water-rich material (making them “wet”).

Another hypothesis is the formation of these small planets on their tight orbits (also known as “in-situ” formation) (Chiang & Laughlin 2013). A planet that formed that closely to its host star would be expected to lack volatiles and be “dry”. Some models predict that only the most refractory elements (i.e., elements which only condense at high temperatures of approximately 1400 K; Wang et al. 2019) would be available as planetary building blocks, leading to the formation of relatively low density, core-less worlds dominated by Calcium and Aluminium (Dorn et al. 2019).

Additional measurements of the radii and masses of USPs, along with discovering more of these planets, will contribute to our understanding of how this population is formed. Certain models offer predictions about their origin, impacting the presence of water they might contain. *JWST* could then be used to characterize the atmospheres of these worlds to search for water. Moreover, models, such as the low eccentricity tidal dissipation scenario (Pu & Lai 2019), make specific predictions about the existence of unseen planets, providing testable hypotheses for future observations.

### 1.1.3 Lava planets

If the temperature on the dayside of a small, rocky exoplanet reaches a temperature of approximately 1300 K, silicates will start melting leading to a molten surface (see Chao et al. 2021, and references within). Between this temperature and the silicate liquidus temperature of approximately 2000 K the magma will consist of a viscous mix of liquid and solid compounds (Hirschmann 2000; Wordsworth & Kreidberg 2022). It is worth noting here that no solar system body experiences temperatures like this caused by solar irradiation with the substellar temperatures of Mercury and Venus being well below 1000 K (Chao et al. 2021). By further increasing the dayside temperature, the planet’s surface magma ocean will outgas a thin rock vapor atmosphere (Schaefer & Fegley 2009; Léger et al. 2011; Miguel et al. 2011; Ito et al. 2015; Kite et al. 2016). At 1500 K the outgassed atmosphere will be very tenuous at a surface pressure of  $10^{-7}$  bar. This further increases exponentially reaching  $10^{-3}$  bar at 2000 K and  $10^{-2}$  bar at 2500 K (Zilinskas et al. 2022). Depending on the temperature of the planet, various species will dominate the atmospheric composition like Na, O, O<sub>2</sub>, SiO, SiO<sub>2</sub>, MgO, and FeO (Schaefer & Fegley 2009; Miguel et al. 2011; Chao et al. 2021; Zilinskas et al. 2022). Of these, the silicon oxides, SiO and SiO<sub>2</sub> are of particular interest as they have spectral features, which should be detectable by the MIRI/LRS instrument on *JWST*: by observing the planet’s emission spectrum, SiO<sub>2</sub> should cause a lowered emission around 7  $\mu\text{m}$  and SiO will be in emission leading to an increased emission compared to a black body around 9  $\mu\text{m}$  (Zilinskas et al. 2022). Observing these features would lead to the first detection of a rocky vapor atmosphere outgassed from a magma ocean. Thankfully, the archetypal lava world K2-141 b will be observed in two separate *JWST* programs during Cycle 1 of its mission: program GO2347 by Dang et al. (2021) and GO2159 by Espinoza et al. (2021).

## 1.2 Observing techniques of atmospheres

In the following, several techniques for the characterization of transiting exoplanets will be discussed (there are many in-depth reviews on exoplanet atmospheres characterization methods and their results; see e.g., Deming & Seager 2017; Kreidberg 2018; Deming et al. 2019; Madhusudhan 2019). Some techniques like direct imaging of exoplanet atmospheres or high-resolution Doppler spectroscopy will not be covered here as the current instruments do not have the needed precision to detect the faint signal caused by rocky exoplanet atmospheres. This is typically because the star outshines its companion by several orders of magnitude, making it challenging to detect the planetary signature. It is however worth noting that high-resolution Doppler spectroscopy on a ground-based extremely large telescope (ELT) might be able to be used in the future to detect an atmosphere on the non-transiting, potentially habitable exoplanet Proxima b (Snellen et al. 2013, 2015; Wang et al. 2017; Birkby 2018). Currently being studied, space-based missions, which would be able to characterize potentially habitable exoplanets include NASA’s *Habitable Worlds Observatory (HWO)* (National Academies of Sciences, Engineering, and Medicine 2021) and ESA’s *Large Interferometer For Exoplanets*

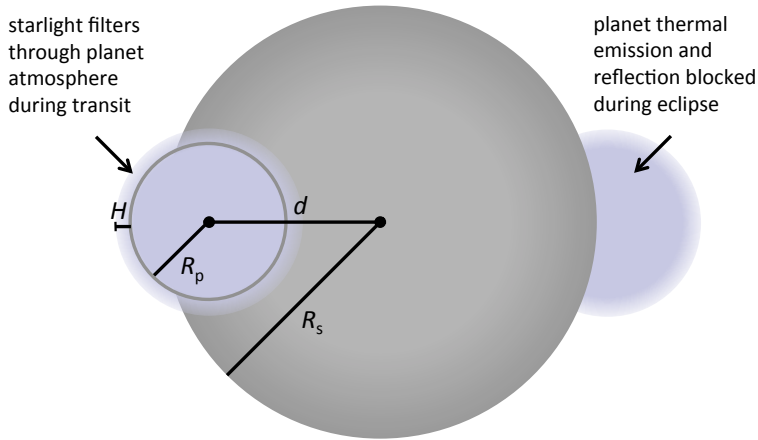


**Figure 1.5:** Geometry of the exoplanetary system when observing a transmission or emission spectrum. When the planet passes between the observer and its host star we observe a transit. Stellar light then travels through the planetary atmosphere, which leads to feature sizes in the transmission spectrum that are proportional to the scale height of the planet  $H = k_B T_{\text{eq}}/(\mu g)$ , where  $k_B$  is the Boltzmann constant,  $T_{\text{eq}}$  the equilibrium temperature of the planet,  $\mu$  the mean molecular weight and  $g$  the planetary surface gravity. Approximately, half an orbital period later, the planet disappears behind its star and we observe the eclipse. Figure adapted from Robinson (2017) and Kreidberg (2018).

(*LIFE*) mission (Quanz et al. 2022b,a).

### 1.2.1 Transmission spectroscopy

When a planet transits between us (the observer) and its host star, the stellar light will pass through the planetary atmosphere at the day-night terminator (see Fig. 1.5). At the moment of transit (also known as primary eclipse) we see absorptions caused by the planet's spectrum superimposed with the stellar spectrum. By taking the difference between the spectrum we observe during transit and the one out of transit, we receive the transmission spectrum of the exoplanet. Molecules or atomic species will then leave absorptions in the transmission spectrum, making them detectable. This technique led to the first detection of an exoplanetary atmosphere on the hot Jupiter HD 209458 using the Space Telescope Imaging Spectrograph (STIS) onboard the *Hubble Space Telescope (HST)* by looking at the absorption by neutral Sodium in the optical (Charbonneau et al. 2002) and atomic Hydrogen in the UV (Lyman  $\alpha$ ) (Vidal-Madjar et al. 2003).

The size of the planet's transmission spectrum is proportional to the planet's scale height,  $H = k_B T_{\text{eq}}/(\mu g)$ , where  $k_B$  is the Boltzmann constant,  $T_{\text{eq}}$  the equilibrium temperature of the planet,  $\mu$  the mean molecular weight and  $g$  the planetary surface gravity. This explains why the best planets for transmission spectroscopy will have high temperatures, low surface gravities, and a low mean

molecular weight atmosphere, e.g., hydrogen-dominated atmospheres. Commonly detected species in transmission spectroscopy include molecules in the infrared wavelengths, like  $\text{H}_2\text{O}$  (e.g., Kreidberg et al. 2015), or now with *JWST*  $\text{CO}_2$  (*JWST* Transiting Exoplanet Community Early Release Science Team et al. 2023) and  $\text{CH}_4$  (Bell et al. 2023b). Furthermore, the alkali metals Na and K can be detected in the visible due to their strong absorptions in the visible (e.g., Charbonneau et al. 2002; Feinstein et al. 2023).

Clouds can also strongly affect the observed transmission spectrum of a planet caused by the slant viewing geometry through the planet’s atmosphere during transit (Fortney 2005; Sing et al. 2016). They effectively make a planet appear bigger and therefore completely mute or weaken spectral features in the transmission spectrum (see e.g., Deming et al. 2013; Kreidberg et al. 2014a; Knutson et al. 2014; Kreidberg et al. 2015). Due to Rayleigh scattering, condensates can also lead to a strong increase in transit depths at shorter wavelengths, causing a so-called scattering slope (see e.g., Pont et al. 2008; Lecavelier Des Etangs et al. 2008; Sing et al. 2011b). Clouds do not weaken planetary features in emission (see Chapter 1.2.2) as much as they do in transmission due to the long slant paths at the limb the photons travel through in the latter technique.

The heterogeneity of the stellar disk can strongly affect a transmission spectrum and has to be considered (Sing et al. 2011b; Rackham et al. 2017, 2018; Pinhas et al. 2018; Rackham et al. 2023). In particular, an unocculted starspot (cool areas on the stellar photosphere) will make the star effectively redder during transit, as more area of the star is cooler than compared to out of transit. This reddening will lead to an increasing slope towards shorter wavelengths in the planetary spectrum McCullough et al. (2014). On the other side, faculae, which are hot spots on a star, will lead to a decrease in transit depth with shorter wavelengths. Additionally, the existence of molecules (like water, Wallace et al. 1995), in a cool star spot can lead to wrongly attributing the molecular features to the planet’s atmosphere (Kreidberg 2018). This effect is known as the transit light source (TLS) effect and is caused by the fact that the transit chord might not be representative of the stellar disk as a whole (Rackham et al. 2018). This is particularly a problem for planets orbiting M dwarfs which are typically more active and have a higher star coverage (Rackham et al. 2018). The TLS effect does not affect emission spectroscopy because the planet does not cross the stellar disk during this kind of observation. The only way to disentangle the planetary and stellar signals is by monitoring the star and determining its activity by studying its photometry variability or comparing to activity indicators (e.g., Nikolov et al. 2014).

### 1.2.2 Emission spectroscopy

Approximately half an orbital period after the transit, we observe the (secondary) eclipse of the planet. The exact timing of the eclipse depends on the eccentricity of the planet and the argument of periastron (for a review on secondary eclipses see Alonso 2018). During the eclipse, we only observe the spectrum of the star because the planet is hidden behind its host star providing us with the measurement of the baseline. Right before and after the eclipse, we see the combined planetary

dayside and stellar spectrum. By taking the difference between these two cases we yield our dayside emission spectrum of the planet which is the spectrum, reflected or emitted by the dayside of the planet. Compared to the transmission spectrum, we now probe the dayside compared to the limb or terminator of the planet.

A planetary emission spectrum will have two contributions: reflection and emission. Reflection typically dominates at optical wavelengths where exoplanet host stars typically reach the peak of their stellar spectrum. Thermal emission on the other side usually dominates in the infrared wavelengths due to the lower temperatures of the exoplanets. The majority of dayside observations have been performed in the infrared as with longer wavelengths the host star is fainter as in the optical, increasing the planet-to-star contrast and making the planet more observable.

The planet’s albedo plays an important role when observing an eclipse: in reflected light which is typically the dominating source of emission coming from a planet in the optical wavelengths, the amount of reflectivity is typically described by the geometric albedo,  $A_g$ . It is basically a measurement of the reflection efficiency of the planet as a function of wavelength at full illumination (i.e., at a phase angle of zero) (Seager 2010; Roberge & Seager 2018). High geometric albedos might be indicative of reflective clouds in the atmosphere, surface ices, or highly reflective lava (see e.g., Mansfield et al. 2019). The thermal emission on the other hand depends on the planet’s temperature. Temperature is connected to the planet’s heat redistribution efficiency and the planet’s Bond albedo  $A_B$ . The Bond albedo measures the fraction of stellar radiation that is absorbed by the planet at all wavelengths and is therefore wavelength independent (Seager 2010; Deming & Seager 2017; Alonso 2018).

The first eclipse observations were observed with the *Spitzer Space Telescope* in the infrared for hot Jupiters (Deming et al. 2005; Charbonneau et al. 2005). For both planets, temperatures were derived by measuring the depth of the eclipse. Furthermore, the timing of the eclipse constrained the eccentricity of the planets. In the following years, *Spitzer* continued to detect many more eclipses of exoplanets in the infrared. The IRAC photometry centered around 3.6 and 4.5  $\mu\text{m}$  became the powerhouse of space-based eclipse and phase curve observations until the telescope’s shutdown in 2020.

The emerging planetary emission spectrum will depend on the chemical composition of the planetary atmosphere and its temperature gradient (Kreidberg et al. 2014b; Stevenson et al. 2014b). A temperature profile with a temperature decreasing with altitude will lead to an absorption feature. For example, a cloud and haze-free,  $\text{CO}_2$  dominated atmosphere will show strong absorption in its planetary emission spectrum at 15  $\mu\text{m}$ . This is because the  $\text{CO}_2$  molecule exhibits a “bending” mode at this wavelength (Catling & Kasting 2017) leading to the gas preventing us from probing the low, hot surface and we only see the cold, top layer of the atmosphere at this wavelength<sup>1</sup>. If the temperature gradient is reversed, the temperature increases with altitude, we will see the  $\text{CO}_2$  in emission. This can for example happen if the atmosphere has hazes that absorb stellar radiation in the

---

<sup>1</sup>The effective absorption of infrared radiation by  $\text{CO}_2$  is also why it is such an effective greenhouse gas in the Earth’s atmosphere (Catling & Kasting 2017).

upper layers of the atmosphere. This will lead to an effective heating of the top atmospheric layer and a cooling of the lower ones. This process is called “thermal inversion” and it is also observed in our solar system: for example, on Earth due to ozone absorbing UV in the stratosphere and on Saturn’s moon Titan due to photochemical hazes (Lellouch 2018; Encrenaz & Coustenis 2018).

Eclipse measurements also give strong constraints on the global climate and heat transport on an exoplanet. In the case of a thick atmosphere, winds can transport heat from the dayside over to the nightside, effectively cooling the dayside and heating the nightside. We therefore get an estimate of the surface pressure by measuring the dayside temperature (Selsis et al. 2011; Koll et al. 2019a). The full picture of a planet’s climate can be revealed by observing the planet’s emission at all planetary phases by observing a so-called “phase curve”.

### 1.2.3 Phase curves

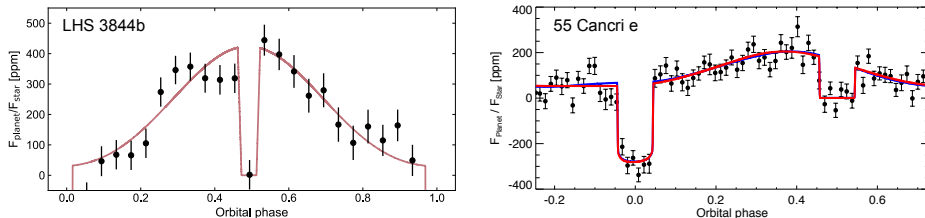


**Figure 1.6:** Thermal phase curves of small ( $< 2 R_{\oplus}$ ) exoplanets as observed by *Spitzer*. Left: The symmetric phase curve of the rocky exoplanet LHS 3844 b ( $1.3 R_{\oplus}$ ) reveals no indication of a hotspot offset, suggesting that the planet is devoid of any atmosphere and resembles a bare rock. Right: The peak emission occurs before the eclipse for the phase curve of 55 Cnc e ( $1.9 R_{\oplus}$ ). This hot spot offset is indicative of heat transport in a moderate mean molecular weight (CO or  $N_2$ ) atmosphere with a surface pressure of a few bars. In this scenario, a super-rotating jet could transport energy away from the substellar point (Kite et al. 2016; Hammond & Pierrehumbert 2017; Angelo & Hu 2017). The hotspot offset could however not be confirmed by a reanalysis of the data by Mercier et al. (2022). Figures taken from Kreidberg et al. (2019a); Demory et al. (2016a); Wordsworth & Kreidberg (2022).

When we observe a planet for a whole planetary orbit, we will measure the planet’s spectrum from the different sides (or phases) of the planet (for a review on phase curves and mapping exoplanets with them, see Parmentier & Crossfield 2018; Cowan & Fujii 2018). By measuring the emission coming from the various longitudes of the planet, we measure the day-to-night temperature contrast informing us about the heat transport on the planet. We essentially measure an emission spectrum at various phases of the planet, giving us information on the abundances and temperatures all around the planet Sing et al. (2016).

The planets that are typically being studied with phase curves are on short orbital orbits of a few days or hours and due to the strong tidal forces they experience most likely tidally locked. Eclipses, which give us a measurement of the

stellar flux alone, provide us with a baseline. Therefore, phase curve observations usually start shortly before an eclipse and end right after the following eclipse, one orbital period later (e.g., Mikal-Evans et al. 2022). As this observational setup also covers at least one transit, we additionally observe a transmission spectrum.

The first successful photometric phase curve was measured by Knutson et al. (2007) for the hot Jupiter HD 189733 b with the *Spitzer Space Telescope* at 8  $\mu\text{m}$ . The peak brightness did not occur at the substellar point but right before the eclipse, indicating an eastward offset of the hotspot. These observations were in agreement with predictions made by 3D global circulation models (GCMs), which were developed to explain the observed thermal hot Jupiter phase curves. These models predict the existence of an eastward equatorial jet transporting heat eastwards away from the substellar point (Showman et al. 2008, 2009). The first spectroscopic phase curve was then taken by Stevenson et al. (2014b) with *HST*/WFC3 for the hot Jupiter WASP-43 b (Kreidberg 2018). The observations were able to constrain the planet’s temperature-pressure profile as a function of longitude, the hotspot offset as a function of wavelength, and with all that unveiling the substantial information content stored in a spectroscopic phase curve observation. Phase curve observations of smaller planets have been also possible thanks to *Spitzer* and *JWST* (see 1.3.1 and 1.3.3).

## 1.3 Notable Planets and Systems

In the following, I will discuss a selection of small exoplanets, that had a successful eclipse measurement in either other optical or infrared, giving us constraints on the planet’s reflectivity or temperature.

### 1.3.1 55 Cnc e

55 Cnc is a bright ( $V = 6$  mag,  $K_s = 4$  mag), nearby (12.6 pc), Sun-like star hosting five exoplanets (for a review on the system, see Fischer 2018). Only the most inner one planet, 55 Cnc e is known to be transiting with an ultra-short-period of 18 hours (McArthur et al. 2004; Fischer et al. 2008). The short orbital period leads to an equilibrium temperature of approximately  $T_{\text{eq}} = 1950$  K (Bourrier et al. 2018) (assuming a Bond albedo of zero and perfect heat redistribution). Transits of the planet were discovered around the same time with the Microvariability and Oscillations of Stars (*MOST*) telescope (Winn et al. 2011) and the *Spitzer Space Telescope* (Demory et al. 2011). The planet’s bulk density ( $R_p = 1.9 R_{\oplus}$ ,  $M_p = 8.6 M_{\oplus}$ ) is inconsistent with an Earth-like interior composition but rather with a pure silicate ( $\text{MgSiO}_3$ ) composition, a composition with a significant amount of volatiles or a composition dominated by Al and Ca without any iron core (Crida et al. 2018b; Zeng et al. 2019; Dorn et al. 2019).

The phase curve captured by the *Spitzer Space Telescope*, which was the first one taken for a small exoplanet, revealed a surprisingly large eastward offset of the planet’s hotspot ( $41 \pm 12^\circ$ ) (see Fig. 1.6) (Demory et al. 2016a). This phase curve offset was initially attributed to a moderate mean molecular weight (CO or  $\text{N}_2$ )

atmosphere with a surface pressure of a few bars featuring a super-rotating jet, which transports energy away from the substellar point (Kite et al. 2016; Hammond & Pierrehumbert 2017; Angelo & Hu 2017). However, a recent reassessment conducted by Mercier et al. (2022) indicated that this hotspot offset might be an artifact of the data reduction process, revealing a negligible offset instead. The eclipse depth of the planet was also found to vary by a factor of 3.7 between 2012 and 2013, corresponding to dayside brightness temperatures ranging from 1300 K up to 2800 K (Demory et al. 2016b). The authors suggested that the observed changes might be attributed to volcanic activity, giving rise to plumes that raise opacity within the *Spitzer* bandpass (Demory et al. 2016b; Tamburo et al. 2018). A recently published optical phase curve of 55 Cnc e observed by *CHEOPS* (CHaracterising ExOPlanet Satellite) detects a phase-curve amplitude and offset that varies in time, potentially attributing it to a dust torus around the star (Meier Valdés et al. 2023).

Even after all the monitoring, the planet’s atmospheric and interior composition is still unclear. The search for escaping hydrogen from the planet led to a non-detection of hydrogen-atmosphere (Ehrenreich et al. 2012). A recent study did also not discover any Helium atmosphere (Zhang et al. 2021b). Both studies together make it unlikely that 55 Cnc e has any H/He-rich primordial atmosphere. The search for various atomic and ionized species that might have originated from a silicate-vapor atmosphere in high-resolution spectroscopy also only led to non-detections (Keles et al. 2022; Rasmussen et al. 2023). A low-resolution *HST*/WFC3 transmission spectrum by Tsiaras et al. (2016a) hinted at an HCN absorption feature in a likely hydrogen-rich atmosphere. High-resolution transit spectroscopy by Deibert et al. (2021) however ruled out the most likely models presented in Tsiaras et al. (2016a). To shed light on 55 Cnc e, two *JWST* programs were approved in Cycle 1 which will characterize the planet’s atmosphere and planetary rotation period (see Fig. 1.4) (Hu et al. 2021; Brandeker et al. 2021).

### 1.3.2 Kepler-10 b

Kepler-10 is an old, fainter ( $V = 11$  mag,  $K_s = 9$  mag) Sun-like star with two transiting (Kepler-10 b and c) and one non-transiting planet (Kepler-10 d) (Bonomo et al. 2023). Kepler-10 b is a lava world with a bulk density consistent with Earth ( $R_p = 1.5 R_\oplus$ ,  $M_p = 3.3 M_\oplus$ ) and an ultra-short orbital period of just 20 hours leading to an equilibrium temperature of  $T_{\text{eq}} = 2170$  K. The planet was the first rocky planet discovered by the *Kepler* mission (Batalha et al. 2011). Eclipse observations of the planet by *Kepler* showed a relatively deep eclipse depth that suggests a high geometric albedo of  $0.60 \pm 0.09$  for the planet (Batalha et al. 2011; Sheets & Deming 2014). This comes as a surprise as small exoplanets ( $1.0 - 2.0 R_\oplus$ ), are typically very dark showing upper values in the geometric albedos of  $0.11 \pm 0.06$  (note that Kepler-10 b is removed from this statistical albedo analysis because it significantly increases the average of the *Kepler* small planet sample) (Sheets & Deming 2017). A high reflectivity like that for Kepler-10 b might be due to clouds or due to unusually reflective lava (Rouan et al. 2011; Essack et al. 2020). How-

ever, recently Zieba et al. (2022) suggested that the high emission in the optical would not be due to a highly reflective surface but rather due to emission features of Sodium and Potassium indicating a silicate atmosphere, which would be consistent with the planet’s bulk density and high dayside temperature. Further spectroscopic follow-up of the planet in these optical wavelengths could confirm this hypothesis.

### 1.3.3 LHS 3844 b

LHS 3844 b was discovered by the Transiting Exoplanet Survey Satellite (*TESS*) and has an orbital period of just 11 hours (Vanderspek et al. 2019). The small planet ( $R_p = 1.3 R_\oplus$ ) has an equilibrium temperature of  $T_{\text{eq}} = 805$  K and is orbiting an M dwarf ( $V = 15$  mag,  $K_s = 9$  mag). The planet was observed for over 100 hours continuously with *Spitzer* at  $4.5 \mu\text{m}$  to collect its thermal phase curve (Kreidberg et al. 2019a). The phase curve was symmetric showing no hint of a hotspot offset (see Fig. 1.6), a large day-nightside contrast, and no significant flux emitted by the planet’s nightside. All that is consistent with the planet being a bare rock and the modelling presented in Kreidberg et al. (2019a) ruled out any thick ( $> 10$  bar) atmosphere on the planet. Thinner atmospheres would have been eroded by the stellar irradiation over the planet’s lifetime. Ground-based transmission spectra are also consistent with no significant atmosphere on the planet (Diamond-Lowe et al. 2020).

The planet is in a sweet spot for surface characterization with the highest expected thermal emission signal among terrestrial planets below 1000 K, without reaching temperatures that would cause surface melting (Mansfield et al. 2019). By comparing the eclipse depth measured by *Spitzer* with emission spectra corresponding to various surface compositions (ultramafic, feldspathic, basaltic, and granitoid), it was determined that the observations are most consistent with a pure dark basaltic surface (Kreidberg et al. 2019a). A surface like this is similar to the lunar mare and Mercury, possibly arising from widespread extrusive volcanic activity. MIRI/LRS eclipse observations scheduled for *JWST* Cycle 1 will measure the infrared emission spectrum of the planet between  $5$  and  $12 \mu\text{m}$  and search for trace amounts of  $\text{SO}_2$  which might arise from volcanic activities (Kreidberg et al. 2021b). A *JWST* phase curve of the planet will be also studied by Zieba et al. (2023a) with NIRSpec/G395H ( $2.87 - 5.14 \mu\text{m}$ ), to study the emission as a function of longitude.

### 1.3.4 TRAPPIST-1

A particularly interesting system for the characterization of rocky exoplanets is TRAPPIST-1 (for a short review on the TRAPPIST survey and TRAPPIST-1, see Burdanov et al. 2018; Gillon et al. 2020). Seven approximately Earth-sized planets orbit the nearby (12 pc) ultra-cool-dwarf ( $M_s = 0.09 M_\odot$ ,  $R_s = 0.12 R_\odot$ ) TRAPPIST-1, with orbital periods ranging from 1.5 days (for planet b) to 18.8 days (for planet h) (Gillon et al. 2016, 2017; Agol et al. 2021). The planets allow us to do comparative planetology between all seven transiting planets in this system

(Morley et al. 2017). Up to four of the planets (d, e, f, g) are also in the temperature zone around their star where liquid water could exist on the planet’s surface, making this system particularly interesting for the study of its habitability (Kasting et al. 1993; Kopparapu et al. 2013, 2014; Wilson et al. 2021). There are several factors contributing to the potential challenges faced by the TRAPPIST-1 planets in retaining their atmospheres, rendering them comparatively less hospitable for life: late M-dwarfs like TRAPPIST-1 have prolonged pre-main sequence phases (Baraffe et al. 1998, 2015), which can take billions of years, where they highly luminous leading to extreme water loss (Luger & Barnes 2015; Bolmont et al. 2017). They are also known to show frequent flares and coronal mass ejections further leading to atmospheric escape (Roettenbacher & Kane 2017; Paudel et al. 2018; Tilley et al. 2019; Airapetian et al. 2020).

The system was observed by *Spitzer* continuously for approximately 20 days in 2016. Due to the compact nature of the system, the system experiences transit-timing variations (TTVs): the planetary transits do not occur in a constant interval but vary due to gravitational interactions between the different planets. The delay or early arrival of a transit depends on the masses of the other planets in the system. This technique was then used to measure the masses and radii of all of the planets in the system to high precision (Yee et al. 2017). The masses are two orders of magnitude more accurate than what current radial velocity (RV) capabilities can achieve (Agol et al. 2021). The planets do all fall onto the same rocky mass-radius relationship which is slightly depleted in iron compared to the Earth, 21% for the TRAPPIST-1 planets compared to 32% for the Earth. Also consistent would be the planets having an Earth-like composition, which is enriched in lighter elements, like water (Agol et al. 2021).

The transmission spectra of all planets in the TRAPPIST-1 system have been collected with *HST*/WFC3 and *Spitzer* but were only able to rule out hydrogen-dominated atmospheres. The observations are all consistent with cloudy atmospheres, high mean-molecular weight atmospheres (e.g., CO<sub>2</sub>, H<sub>2</sub>O), or no atmospheres at all (de Wit et al. 2016, 2018; Zhang et al. 2018; Ducrot et al. 2018; Garcia et al. 2022). All of the planets will be studied by *JWST* in Cycle 1 in transmission and the two most inner planets, b and c, in emission. The first *JWST* transmission spectrum of a TRAPPIST-1 planet was published in Lim et al. (2023), which used *JWST*/NIRISS (0.6 – 2.8  $\mu$ m) to observe planet b in two visits. The shape of the transmission spectra between the two visits differs significantly from each other which is explained by unocculted starspots in the first visit and unocculted faculae in the second. The observations were able to rule out hydrogen-rich atmospheres confirming previous studies, but could not determine the atmospheric composition. The study shows how stellar contamination dominates over the transmission spectrum and that the stellar contribution has to be accurately disentangled from the planetary signature. As discussed in Section 1.2.2, emission spectroscopy does not suffer from stellar contamination like transmission, because the planet does not move across the stellar disk as seen by the observer, therefore not occulting any star inhomogeneities. The photometric emission studies of TRAPPIST-1 b (Greene et al. 2023) and TRAPPIST-1 c (Zieba et al. 2023b) with *JWST* showed deep eclipses at 15  $\mu$ m. They are inconsistent with cloud-free, CO<sub>2</sub> dominated

atmospheres as the  $\text{CO}_2$  in their atmospheres would lead to low brightness temperatures at  $15\ \mu\text{m}$  and therefore shallow eclipses. TRAPPIST-1 b is consistent with a dark, bare rock surface, whereas TRAPPIST-1 c is more consistent with thin  $\text{CO}_2$  atmospheres are slightly non-zero albedo surfaces (Greene et al. 2023; Zieba et al. 2023b). Observations in other wavelengths (outside of the  $\text{CO}_2$  band at  $12.8\ \mu\text{m}$  for planet b, Lagage & Bouwman 2017) and a phase curve (at  $15\ \mu\text{m}$  for planet b and c, Gillon et al. 2023) are planned and will give us a more complete picture of the atmospheres of the planets and their heat redistribution.

## 1.4 Facilities

The majority of detections mentioned in the previous chapters have been primarily focused on the characterization efforts performed with space-based observatories, in particular, *HST*, *Spitzer*, and *JWST*. Ground-based atmospheric characterization has several disadvantages: it for example suffers from turbulence in Earth's atmosphere. There are also wavelengths in particular in the UV and infrared (due to the water absorption bands) where the Earth's atmosphere is mostly opaque and does not let the majority of radiation reach the surface. The thermal background is also higher on Earth than in a thermally stable environment like the Earth-Sun Lagrange point, L2 (where *JWST* is located). On the other side, however, ground-based telescopes are theoretically not space-constrained, unlike space telescopes, which must conform to the dimensions of the launch rocket fairing. Ground telescopes have detected, for example, Na and K in the optical wavelengths (e.g., Redfield et al. 2008; Snellen et al. 2008; Sing et al. 2011a), Helium (e.g., Allart et al. 2019; Zhang et al. 2022), water (e.g., Birkby et al. 2013) or various carbon and nitrogen-bearing species (e.g., Jacobbe et al. 2021).

Figure 1.7 shows a selection of space-based instruments for the study of exoplanets. Of these the powerhouse facilities of atmospheric characterization in the past decade were *HST* with its WFC3 (Wide Field Camera 3, covering the near-infrared) (McCullough & MacKenty 2012; Deming et al. 2013) and STIS (Space Telescope Imaging Spectrograph, covering the optical and UV) (Ehrenreich et al. 2015; Sing et al. 2016) instruments and *Spitzer* with its photometric Infrared Array Camera (IRAC) Channel 1 and 2 centered around  $3.6$  and  $4.5\ \mu\text{m}$  (Fazio et al. 2004). The WFC3 G141 grism ( $1.1$  and  $1.7\ \mu\text{m}$ ) covers a strong water absorption feature around  $1.4\ \mu\text{m}$ , which leads to dozens of detections of water in the atmospheres of hot Jupiters, Neptune-sized planets, and sub-Neptunes (e.g., Deming et al. 2013; Huitson et al. 2013; McCullough et al. 2014; Fraine et al. 2014; Kreidberg et al. 2014b, 2015; Benneke et al. 2019). By observing eclipses, *HST* also detected the same water feature in emission in the atmosphere of some exoplanets (e.g., Crouzet et al. 2014; Kreidberg et al. 2014b). G102, the bluer grism on *HST*/WFC3 was used to detect Helium in the atmosphere of WASP-107 at  $1083\ \text{nm}$  (Spake et al. 2018). Finally, STIS has led to many Na ( $577\ \text{nm}$ ) and K ( $779\ \text{nm}$ ) detections in the atmospheres of transiting hot Jupiters (Sing et al. 2016; Madhusudhan 2019). Additionally to the high precision spectroscopy by *HST*, the *Spitzer* Space Telescope has been able to provide us with near-continuous pho-

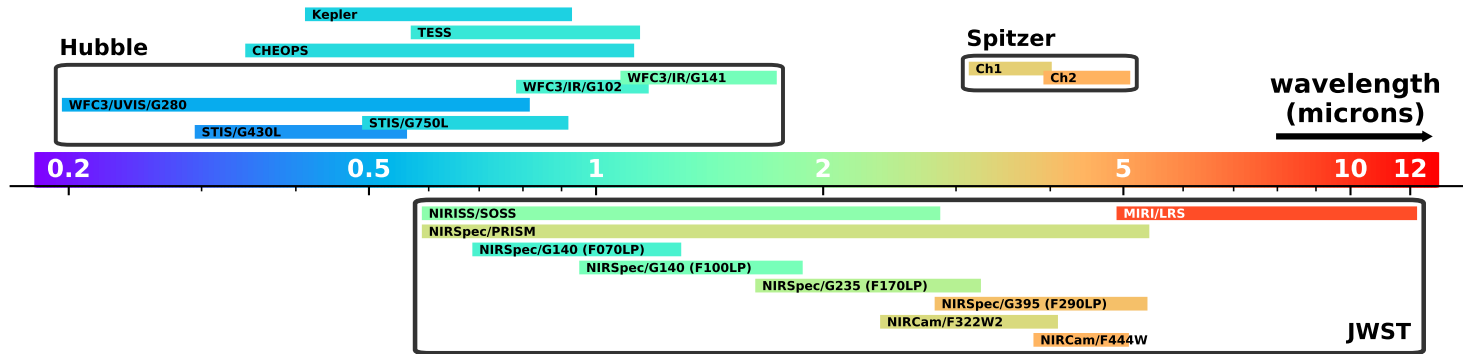


**Figure 1.7:** Figure showing current (*JWST*, *HST*, *TESS*, and *CHEOPS*) and past (*Kepler* and *Spitzer*) space-based instruments and telescopes for the observation of exoplanets and their coverage of the electromagnetic spectrum. Other observational modes of *HST* or *Spitzer* are not depicted, as they were either only used on a handful of planets (e.g., Channel 3 and 4 on *Spitzer*, which were operational in the telescope’s “cold phase”) or generated not reproducible results (e.g., the NICMOS instrument on *HST*). Next to *JWST*’s MIRI/LRS instrument (low-resolution spectrograph; approximately 5 – 12  $\mu\text{m}$ ), MIRI also has nine broadband filters for photometric imaging with their center wavelength ranging from 5.6 to 25.5  $\mu\text{m}$ . See Zieba et al. (2023b) i.e., scientific chapter 4, for an application of MIRI filter F1500W (centered around 15  $\mu\text{m}$ ) to observe an exoplanet. There is also a prospect of using MIRI/MRS (medium-resolution spectrograph; ranging from approximately 5 to 28  $\mu\text{m}$ ) for transiting exoplanets (Deming et al. 2021). Only *JWST* and *HST* have spectrographs. *Kepler*, *TESS*, *CHEOPS*, and *Spitzer*’s IRAC Channels 1 and 2 are photometric. Figure adapted from Kreidberg (2018).

tometry observations in its “warm phase” (after its coolant ran out) until it shut down in 2020, leading for example to phase curve observations of rocky exoplanets or the characterization of the TRAPPIST-1 planets (for a review of the scientific highlights of *Spitzer*, see Deming & Knutson 2020).

Following the deployment of the *James Webb Space Telescope (JWST)* on December 25th, 2021, followed by the start of scientific data collection, a state-of-the-art space telescope has been introduced, enhancing our observational capabilities. The advantages of *JWST* are immense, most importantly (1) *JWST* collecting area is approximately 6 times greater than *HST*’s collecting area, and (2) the various instruments cover a great wavelength range from the optical at 0.6  $\mu\text{m}$  up to 28  $\mu\text{m}$  (although the longest wavelengths might not be usable for transiting exoplanets) (see Fig. 1.7). In the short time of its operations, it has already delivered major discoveries for transiting exoplanets including the first detection of  $\text{CO}_2$  (*JWST* Transiting Exoplanet Community Early Release Science Team et al. 2023),  $\text{CH}_4$  (Bell et al. 2023b), and  $\text{SO}_2$  (*JWST* Transiting Exoplanet Community Early Release Science Team et al. 2023; Rustamkulov et al. 2023; Alderson et al. 2023) in an exoplanet atmosphere, the first detection of photochemistry following the observation of  $\text{SO}_2$  (Tsai et al. 2023), and the first detection of thermal emission coming from temperate rocky exoplanets (Greene et al. 2023; Zieba et al. 2023b). Anticipating a propellant lifespan of 20 years or beyond for *JWST*, it is expected that its observations will lead to numerous groundbreaking discoveries that will improve our understanding of exoplanets and their atmospheres (Rigby et al. 2023).

## 1.5 This thesis

The work in this thesis revolves around the characterization of exoplanets through the analysis of primarily space-based data. Even though I do not spatially resolve the planet from the star in any of these following works, the combined stellar and planetary light informs us about the properties of the exoplanet like its radius, atmospheric composition, reflectivity, and heat redistribution. The photometric and spectroscopic observations were taken with a range of telescopes like *Kepler*, *Spitzer*, *HST*, and *JWST*.

In **Chapter 2** we characterize a lava world called K2-141 b with an ultra-short orbital period of just 6.7 hours. Discovered by *Kepler* during its second-light K2 mission, the planet showed a strong eclipse signal in the optical wavelengths of *Kepler*. By only having this one emission measurement, however, we have a degeneracy: we do not know how much of this emission is due to reflection and how much is due to thermal emission. We therefore study approximately 70 hours of *Spitzer* photometry of the planet in the infrared at 4.5  $\mu\text{m}$ . With these continuous observations, we are able to take its phase curve and measure a hot dayside and cold nightside, consistent with no thick atmosphere redistributing heat. We also break the degeneracy by combining the optical data of *Kepler* and the infrared data of *Spitzer* and show that the high emission in the optical is either due to a reflective surface or emission features caused by a rock-vapor atmosphere. We also

suggest that the latter process might explain the high observed emission seen for Kepler-10 b rather than a reflective surface.

In **Chapter 3** we published an open-source `Python` code called `PACMAN`. It is an end-to-end pipeline for *Hubble Space Telescope* (*HST*) data taken by either of the infrared grisms on the Wide-Field-Camera 3 (WFC3). It includes spectral extraction and light curve fitting to receive a planetary transmission or emission spectrum. Covering a strong water absorption feature at  $1.4\ \mu\text{m}$  and its high stability and precision, which has been also used to observe phase curves of exoplanets, *HST* remains a valuable telescope for atmospheric characterization even in the era of *JWST*. In Chapter 5, we present the analysis of *HST*/WFC3 data for a hot, sub-Saturn mass planet using `PACMAN`.

In **Chapter 4** we present one of the first studies using data from the long-awaited *James Webb Space Telescope* (*JWST*). We use the Mid-Infrared Instrument (MIRI) on *JWST* combined with the  $15\ \mu\text{m}$  filter to observe the thermal emission coming from the temperate planet TRAPPIST-1 c. Our measured brightness temperature is disfavoured a thick,  $\text{CO}_2$ -rich cloud-free atmosphere on the planet. The observations are able to rule out cloud-free  $\text{O}_2/\text{CO}_2$  mixtures with surface pressures ranging from 10 bar (with 10 ppm  $\text{CO}_2$ ) to 0.1 bar (pure  $\text{CO}_2$ ). Thinner atmospheres or bare-rock surfaces are consistent with our measured planet-to-star flux ratio. The absence of a thick,  $\text{CO}_2$ -rich atmosphere on TRAPPIST-1 c suggests a relatively volatile-poor formation history, for the planet. If all planets in the system formed in the same way, this would indicate a limited reservoir of volatiles for the potentially habitable planets in the system. Shortly before the publication of our work, the innermost planet TRAPPIST-1 b was observed in the same observational mode revealing a deep eclipse consistent with the planet being a dark, bare rock. More data for both planets is needed to paint a more complete picture of them, but already these first observations are presenting *JWST* capabilities to characterize temperate rocky exoplanets and push down to planets in temperature and size to the inner solar system bodies.

In **Chapter 5** we analyze *HST*/WFC3 data of the hot, low-density, sub-Saturn called KELT-11 b. Previous work on the planet using the G141 grisms data ( $1.1 - 1.7\ \mu\text{m}$ ) reveals a low-amplitude water feature that was several orders of magnitude below the anticipated levels predicted by planet formation models on our solar system. In this chapter, we analyze unpublished *HST*/WFC3 G102 ( $0.8 - 1.1\ \mu\text{m}$ ) spectroscopic grism data and also perform a reanalysis of the *HST*/WFC3 G141 data. We show that the previously seen low metallicity might be due to the `divide-white` technique which assumes that systematics do not change with wavelength. The transit depth of our G102 spectrum decreases toward shorter wavelengths, suggesting the presence of faculae on the stellar photosphere influencing our spectrum. This is commonly observed for late-type M-dwarfs but not for earlier-type stars like KELT-11, which is a retired A star. This suggests that stellar inhomogeneities should also be taken into consideration for earlier type stars.

Finally, in **Chapter 6** we work on the  $\beta$  Pictoris system, a near planetary system with gas giant planets, an edge-on circumstellar disk, and transiting exocomets. The star, exhibiting stellar pulsations, particularly  $\delta$  Scuti pulsations,

offers the potential for indirect detection of gas giant planets through time delays in the pulsational signals. Analysis of multi-year  $\delta$  Scuti pulsations using BRITe-Constellation, bRing, ASTEP, and *TESS* data reveals significant pulsations, but the study fails to detect expected signals for  $\beta$  Pictoris b and c. The limitations are attributed to inherent pulsational mode drifts and insufficient sensitivity in combined datasets for detecting timing drifts. Future work might show possible detection limits of other planets in the system.

With this we finish the introduction, covering the exoplanet zoo, detection methods, notable planets, and a short summary of the individual chapters of the thesis. Thanks to the launch of *JWST* and the construction of the ELTs, we will further characterize rocky worlds and compare our solar system to other exoplanetary systems. Of particular interest is also the observation of lava worlds with molten daysides, as the cover temperature regimes which are not accessible in our Solar System. Studying their atmospheres will also further inform us about the interior composition of these worlds. Rocky bare rocks also give us the possibility to study their surface compositions and learn about their geophysical history. Even though we will have to be very lucky to even detect biosignatures in one of the most observable exoplanets, the chances are good in the next few decades with the advent of the ELTs, the *HWO*, or *LIFE*.